Energy Equip. Sys./ Vol. 7/No. 4/Dec. 2019/ 353-375

ENERGY EQUIPSYS

Energy Equipment and Systems

http://energyequipsys.ut.ac.ir
www.energyequipsys.com

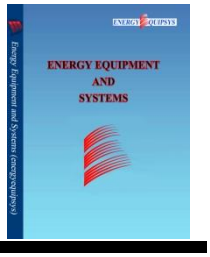

Experimental investigation of bubble growth and detachment in stagnant liquid column using image – based analysis

Authors

Erfan Kosari [a*]
Javad Eshrgahi [b]
Wael H. Ahmed [c]
Pedram Hanafizadeh [b]

[a] Department of Mechanical Engineering, University of California, Riverside, CA 92521, USA

[b] Center of Excellence in Design and Optimization of Energy Systems, School of Mechanical Engineering, College of Engineering, University of Tehran, Tehran, Iran

[c] School of Engineering, University of Guelph, Guelph, Ontario, Canada

Article history:

Received : 10 October 2019
Accepted : 1 December 2019

ABSTRACT

An experimental study has been carried out to characterize bubble formation, growth, and detachment mechanisms in a stagnant liquid column. Both bubble frequency and bubble detachment size were measured in different gas flow rates, injector diameters and orientations, submergence height, and liquid properties. Experiments were performed for air injection flow rate ranges between 200 mlph and 1200 mlph using needle diameters of 1.6, 1.19, 1.07, and 0.84 mm submerged in liquids with viscosities of 0.001, 0.1, 0.35, and 1 Pa.s. The data for bubble formation was obtained using a high-speed imaging technique. The results show that the bubble diameter at the departure increases as the needle diameter, liquid viscosity, and gas flow rate increase. In addition, the decrease in the submergence height results in a larger bubble at the departure. In order to analyze the changes in bubble detachment characteristics, a force modelling on a growing bubble was proposed. The experimental data were utilized for training a feed-forward back propagation neural network system to estimate the bubble detachment diameter. They were also used to propose a correlation to predict bubble diameter at the departure. The proposed correlation is found to be in the range of ± 8% of the obtained experimental data.

Keywords: Bubble Growth, Bubble Detachment Characteristics, Bubble Diameter Correlation, Neural Network.

1. Introduction

The formation, growth, and departure of the bubbles in liquid columns are essential in many industrial applications and flow measurement systems [1]–[3]. One of the most important bubble formation applications is in bubble columns that efforts were carried out to predict the overall flow field in these columns [4]–[6]. Industrial equipment is designed using two-phase hydrodynamic parameters and the bubble generation mechanism to meet the desired performance of different processes. These parameters include the discrete phase characteristics (bubble rise velocity, bubble size) and the liquid properties (surface tension, density, and viscosity) as well as the flow pattern.

The previous studies on single bubble formation are summarized by Tate [7]. Generally, useful parameters are classified into three major groups: liquid characteristics, gas properties and orifice orientation. The complicated nature of

* Corresponding author: Erfan Kosari
Department of Mechanical Engineering, University of California, Riverside, CA 92521, USA
Email: erfan.kosari@gmail.com

bubble growth persuaded researchers to employ experimental techniques for their investigations in this area. In the case of operating conditions, researchers apply two conventional methods for injecting gas into the liquid column to generate bubbles in their experiments: constant pressure gas flow [8]–[10], and constant gas flow rate [11]. Besides the experimental efforts, some authors identified the exact quantitative effects of fundamental parameters on detachment characteristics of bubbles numerically [12], [13]. In a comprehensive study done by Oguz and Prospretti [14], the authors showed the existence of two different bubble growth regimes according to a critical gas flow rate by a simple theoretical model and compared the results with the experiment.

Leibson et al. [15] introduced practical parameters such as viscosity, surface tension, density, and liquid column height as the most effective liquid properties on bubble growth based on experimental studies. Studies in this area have been implemented in a wide range of gas flow rates and orifice diameters. These observations have resulted in different reports which are contradicting in some cases and can be summarized in this way: (I) weak viscosity effect on bubble sizes (II) independency of bubble sizes from liquid viscosity [15], [16] (III) increasing in size of bubbles with liquid viscosity [17]. Furthermore, the quantitative analysis of Jamialahmadi et al. [18] shows that the bubble size depends on dynamic viscosity to the power of 0.66. Similarly, there are apparent contradictions in the reports on the liquid density effects. Khurana and Kumar [8], [17] discovered that increasing in liquid density caused bubble volume decrease for low liquid viscosity and gas flow rates. In addition, the bubble volume is independent of the density of liquid when: (a) viscosity and injector diameter are both small, (b) the viscosity is small and the flow rate is large, in the case of small injectors. These authors also reported that for lower submergence height from the tip of the orifice to the top of the liquid column, bubbles with higher volume were formed.

In addition, limited literature has been devoted to considering the effect of gas properties (such as surface tension and gas density) on bubble formation [19]–[22]. Moreover, Davidson and Amick [23] reported at relatively low flow rates (0.01 – 1 ml/s), the volume of bubbles was proportional to the surface tension and orifice diameter (0.034 – 1.58 cm) and independent of gas flow rate. By injecting different gases into the liquid column, gas density and surface tension effects on the bubble volume have been studied comprehensively by Idogawa [22] and Wilkinson [24]. In work done by Hanafizadeh et al. [25], gas properties effects on bubble growth were analyzed. They reported the volume of bubbles is a strong function of the surface tension and the gas density. The authors also concluded the bubble generation frequency was a strong function of the contact angle and the surface tension.

One of the most important injector parameters that control the bubble diameter is the orifice diameter. Therefore, along with the mentioned parameter, some other governing parameters which affect the bubble formation are orifice chamber volume, the submergence of the orifice, orifice type, orifice material, etc.[26]–[28]. On the contrary, Davidson and Schuler [29] claimed the dimensions of the orifice were of minor importance in bubble detachment size. They formed bubbles of gas in different liquids and they concluded the volume of the bubble that detached was a function of gas flow rate (0 – 50 ml/s) and the viscosity of the liquid. A detailed review of the literature up to 1968 is given by Ramakrishnan et al. [30]. This study concluded positive effects for viscosity at high airflow rates (20 – 80 ml/s) and surface tension at low rates (0 – 20 ml/s). In addition, they reported positive effects on bubble volume partly because of orifice diameter (0.1378 – 0.7042 cm) for viscous and inviscid liquids.

In a more comprehensive study done by Iliadis et al. [31], the authors identified the effective parameters that have considerable impacts on bubble formation for different ranges of gas flow rates of 0.75 – 56.7 ml/s, chamber volumes of 150 – 7000 ml, orifice diameters of 1.15, 2.1, 3.25, and 4.35 mm, and orifice submergence of 0.1 – 1.5 m. They presented their results based on different bubble regimes; in the regime of single bubble formation: the bubble volume increased with the orifice submergence, and in the bubble group formation: the bubble volume was independent of the orifice submergence. These results are in contrast to the submergence height effects of Khurana and Kumar [17] research. In the case of injection system type, Vafaei et al. [32] compared bubble formation from a substrate nozzle immersed in water with the formation

of bubbles from needle nozzles under the same conditions experimentally. They claimed the bubble expansion rate was larger for the substrate than the needle and as a result, the final bubble volume was similar in both cases. Houshmand et al. [33] studied the effect of injection angle, gas flow rate, and liquid flow rate on the bubble formation process in microchannels.

It is concluded from the above articles there is no general consistency to identify the key parameters that can be effective on single bubble formation or detachment. Therefore, a survey of available literature indicates a shortage of comprehensive investigation of bubble formation, which many studies reported some parameters as effective parameters [30], and many others neglected the importance [34], [35]. Also, in a few recent studies, the authors claimed that the mechanism for bubble departure is not balanced of vertical forces i.e. the historical point-force models, and it is due to bubble shape; in the sense that for a given Bond number, there is a critical volume beyond which bubbles can no longer exist in mechanical equilibrium [27], [36]–[38]. In addition, there is no comprehensive comparison between horizontal and vertical injection systems. Hence, more experimental investigations are required to characterize the bubble formation process.

Present investigation aims to analyze the discrepancies in the reported data on bubble size in gas-liquid systems and present new experimental results on the effect of needle size (with a diameter range of 0.84 – 1.6 mm) on bubble volume and bubble frequency for medium range of gas flow rates: 200 – 1200 mlph. Also, to determine the viscosity effects (0.001 – 1 Pa.s) on bubble formation and detachment, the effects of this parameter will be analyzed using Silicon oil. The air is injected into the liquid column at a constant flow rate with different submergence heights. Experiments will be performed for both horizontal and vertical needles to understand the submergence type effects on bubble properties. Furthermore, to achieve a better understanding of bubble growth mechanism, a force modelling on a growing bubble is presented. In this investigation, the feed-forward back propagation neural network design is applied to predict the equivalent bubble detachment diameter. Finally, the experimental data are utilized to develop a parametric correlation for the bubble detachment diameter prediction. The proposed correlation is compared with the most cited correlation [18] in which the effects of submergence height have not been considered while the proposed correlation is taking this effect into account.

Nomenclature

$d_{B,det}$	$Departure\ bubble\ diameter.m$
d_O	$Orifice\ diameter.m$
D_n	$Needle\ diameter.m$
P_g	$Inside\ bubble\ pressure.Pa$
P_l	$Lquid\ pressure.Pa$
h	$Liquid\ height.m$
p	$Needle\ circumference.m$
g	$Gravitational\ acceleration.ms^{-2}$
Q	$Gas\ flow\ rate.m^3s^{-1}$
f	$Bubble\ generation\ frequency.Hz$
h_{det}	$Height\ of\ bubble\ at\ departure.mm$
t	$Time.s$
t_{det}	$Bubble\ generation\ period.s$
C_D	$Drag\ coefficient$
F_B	$Buoyancy\ force.N$
F_P	$Contact\ pressureforce.N$
F_D	$Drag\ force.N$
F_σ	$Surface\ tension\ force.N$

Greek symbols

ρ_L	$Liquid\ density.Kg.m^{-3}$
μ_L	$Liquid\ dynamic\ viscosity.Pa.s$
σ	$surface\ tension\ of\ water\ in\ contact\ with\ air.Nm^{-1}$
ρ_g	$Gas\ density.Kg.m^{-3}$

Dimensionless symbols

$$Bond\ number = Bd = \frac{\rho_L g {d_O}^2}{\sigma}$$

$$Froude\ number = Fr = \frac{16Q^2}{g\pi^2 {d_O}^5}$$

$$Galileo\ number = Ga = \frac{g{\rho_L}^2 {d_O}^3}{{\mu_L}^2}$$

$$Dimensionless\ diameter = \frac{d}{d_{B,det}}$$

$$Dimensionless\ height = \frac{h}{h_{det}}$$

$$Dimensionless\ time = \frac{t}{t_{det}}$$

2. Experimental apparatus and operating conditions

The experimental apparatus used in this study comprises a square liquid column (1),

a syringe pump (2), illumination tools consisting of halogen lamp and softbox (5), standard needles for injection (6 or 7), and a high-speed camera (3) connected to a computer laptop (4), as illustrated in Fig. 1. The bubbles are formed in a square column made from PMMA with dimensions of 100 mm × 100 mm × 300 mm, which is open to the atmosphere at the top. The square column is used conveniently for visual and photographic observations and the sidewall effects are negligible.

During the experiment, air is injected into the column through two different needle orientations: vertical and horizontal. Specifically, the lateral and bottom sides of the column are equipped with some instruments and joints to inject air into the liquid phase under constant flow conditions. The bubbles grow and depart from the needles with diameters of 0.84 mm, 1.07 mm, 1.19 mm, and 1.6 mm in distilled water and three different silicon oils with viscosities of 0.1, 0.35, and 1 Pa.s. The injection system is composed of a needle connected to a syringe pump (AMPall SP8800). The syringe is filled with ambient air and the flow rate is set to produce only a single bubble at a time in the middle of the column. The flow rates chosen for this study are 200, 400, 800, and 1200 mlph. All experiments are conducted under the atmospheric condition and terrestrial gravity. The range of operating parameters covered during the present investigation and other detailed information about the apparatus is summarized in Table 1.

Since having high-quality images is fundamental to this work, a high-speed camera is used to visualize bubble departure around the tip of the needle. A halogen lamp is applied to provide appropriate illumination for high-speed photography. The lamp is placed about a half meter far from the backside of the column. The frame rate, the shutter speed, and aperture value are set according to environmental illumination conditions and the bubble growth rate.

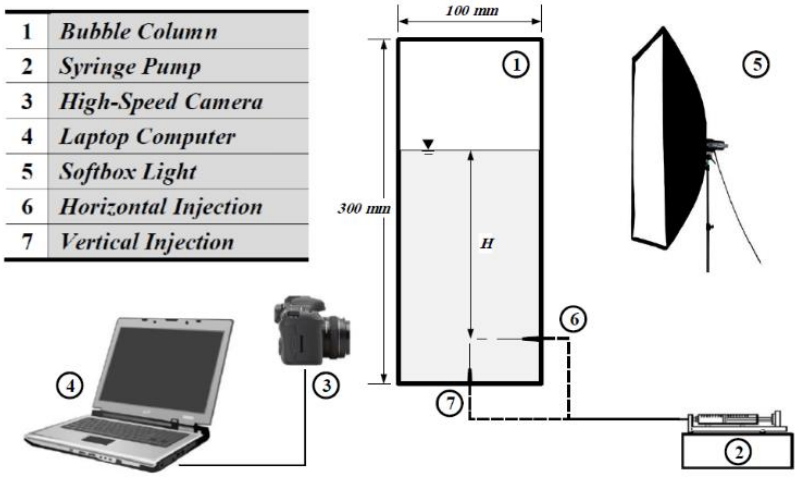

Fig.1. Experimental Apparatus

Table 1. Range of operating parameters

Operating Parameters		Parameter value
Flow rate		200, 400, 800, 1200 mlph
Needles (Inner diameter)		G14 (1.6 mm), G16 (1.19 mm), G17 (1.07 mm), G18 (0.84 mm)
Liquid height		50, 100, 150 mm
Liquid properties	Surface tension ($N.m^{-1}$)	72.5×10^{-3}
	Liquid viscosity (Pa.s)	0.001
Air density		1.15 $kg.m^{-3}$
Morton number		2.6×10^{-12}
Bond number		0.07 – 0.30

The images are captured in the high-speed mode with frame rates ranging between 60 fps to 1200 fps. In the photography mode of 1200 fps, each image contains 336 × 96 pixels. All captured images are then analyzed with a developed routine in MATLAB in order to obtain required bubble characteristics such as bubble volume, the instantaneous contact angle, bubble generation frequency, bubble interface position, and the 3D shape of bubbles for the study. Sequences of recorded high-speed images are processed by the digital image processing method, such as grayscale image, image noise remove, binary image transform, bubble filling, and so on (Fig. 2).

By locating the bubble boundary, a data processing MATLAB code is utilized to define the equation of the circumference passing through the generic point and its neighboring points. Also, this equation is used to determine the bubble contact angle and reconstruct the 3D bubble. 3D bubbles are generated assuming axisymmetry and simply revolving the bubble boundary points about the central vertical axis. The data presented here contain several sources of uncertainty, such as image processing analysis, measurement of airflow rate, and liquid height. In this study, it is assumed that the flow rate is constant during the bubble generation process. The uncertainty magnitude of the airflow rate is approximately 2 – 3 %. However, this error is negligible in the current setup, hence not considered. The instrument used for the liquid height measurement has an accuracy of 0.5 mm (Table 2). In the procedure of image processing, even successive measurements under identical operating conditions result in small changes in the outcomes. Thus, it is concluded that the image processing uncertainties consist of physical calibration and image calibration scale. Physical calibration in image processing is done utilizing measuring the needle's outer diameter which has an accuracy of 0.005 mm. The other uncertainty source of image processing is attributed to the image calibration scale, which has an accuracy of one pixel. Finally, it must be noted that the uncertainties of liquid physical properties and orifice dimensions are not considered in this uncertainty analysis.

3. Force modelling

In this section, a theoretical model based on force balancing is presented by considering the following assumptions:

- The gas momentum force is insignificant compared with other forces acting on the bubble.
- Bubble growth happens adiabatically and axisymmetrically.
- The liquid phase is quiescent and subsequently, the liquid trust force is not taken into account.
- The air pressure within the bubble is uniform, and gas viscous and inertia effects are negligible.
- All gas and liquid phases' properties are assumed to be constant and measured at room temperature.

Fig. 2. Sequence of image processing: (a) original image (b) inverted image, (c) binary image (d) filled binary image, and (e) edge detected image (without smoothing)

Table 2. Uncertainty of the measured variables

Parameter	Amount of uncertainty
Air flow rate	2 – 3 %
Liquid height	0.5 mm
Physical calibration scale	0.005 mm
Image calibration scale	1 pixel

In the process of bubble growth, the forces that hold the bubble to the needle (negative) are larger than the forces that pull the bubble from the needle (positive) when the bubble is very small. As the bubble grows, the positive forces grow faster than the negative forces, until the total force becomes positive and pulls the bubble up (detachment time). The surface tension and drag are the negative forces and buoyancy, and contact pressure is the positive forces which are indicated in Fig. 3. The bubble departure can be determined by a force balance as given by

$$m_g a_{CM} = F_\sigma + F_D + F_B + F_p \quad (1)$$

where F_B, F_p, F_D, and F_σ are buoyancy, contact pressure, drag, and surface tension forces, respectively.

The surface tension force, F_σ, is caused by the attraction of the liquid to the surface that acts around the perimeter of the bubble base. The surface tension force is proportional to the fluid surface tension, σ, and the contact angle, θ according to

$$F_\sigma = \sigma P sin\theta \quad (2)$$

where P is the needle circumference. When the bubble is growing in a viscous fluid, it will be subjected to drag force. In the calculation of drag force, it is also assumed that the bubble is spherical. The drag force is given by

$$F_D = \frac{1}{2}\rho_l C_D u_{CM}^2 \left(\frac{\pi D^2}{4}\right), \quad (3)$$

where ρ_l is liquid density, u_{CM} is rising bubble center of mass velocity, D is the equivalent diameter of the bubble by assuming a spherical shape, and C_D is drag coefficient that can be calculated by Morrison correlation [39] for a wide range of Reynolds numbers, which is given by

$$C_D = \frac{24}{Re} + \frac{2.6\left(\frac{Re}{5.0}\right)}{1+\left(\frac{Re}{5.0}\right)^{1.52}} + \frac{0.411\left(\frac{Re}{263.000}\right)^{-7.94}}{1+\left(\frac{Re}{263.000}\right)^{-8.00}} + \left(\frac{Re^{0.80}}{461.000}\right), \quad (4)$$

where the Reynolds number is defined as

$$Re = \frac{\rho_l u_{CM} D}{\mu_l}, \quad (5)$$

where μ_l is liquid viscosity. For the spherical bubble submerged in the stagnant fluid, the buoyancy force is equal to the weight of the fluid displaced. That is

$$F_B = \frac{\pi D^3}{6}(\rho_l - \rho_g)g, \quad (6)$$

where ρ_g is the density of the gas phase. Finally, the contact pressure force is obtained from

$$F_p = (P_g - P_l)\frac{\pi D_n^2}{4}, \quad (7)$$

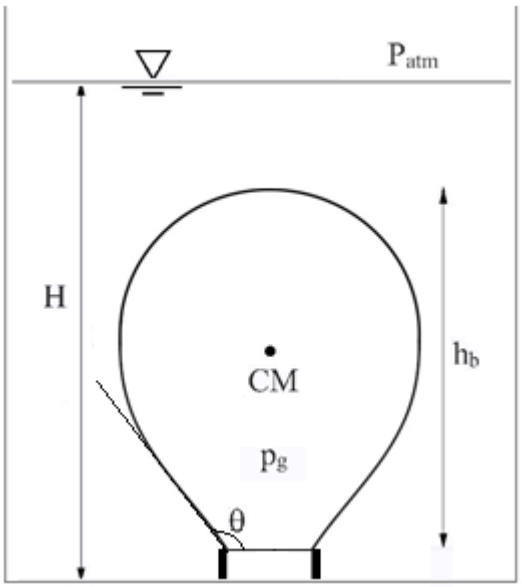

(a)

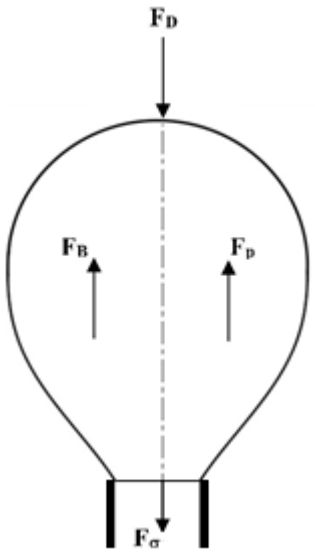

(b)

Fig.3. Bubble schematic (a) overview (b) active forces during bubble growth

where D_n is the needle diameter, P_g and P_l are inside bubble pressure and the liquid pressure value. Applying the Young-Laplace equation:

$$P_g - P_l = \frac{4\sigma}{D} \quad (8)$$

the contact pressure force is given by

$$F_p = \frac{\pi\sigma D_n^2}{D}, \quad (9)$$

where σ is the surface tension of water in contact with air. It should be noted that ρ_l, ρ_g and σ are liquid and gas physical properties measured at room temperature (20°C).

4. Results and discussion

4.1. Bubble formation of needle G14 in water

A typical photographic time sequence of bubble formation from the needle is shown in Fig. 4. The bubble evolution consists of three primary stages. During the first stage, the bubble is emerging from the needle and its shape is that of a spherical segment (Growth stage). When the bubble becomes large enough, it becomes more elongated as a buoyancy force tends to lift the upper portion of the bubble with the bottom remaining fixed to the needle tip, then evolves symmetrically from a spherical shape to an inverse teardrop shape (Necking stage). As liquid circulates inward at the level of the opening, the bubble is detached by a combination of buoyancy force and motion of the liquid toward the opening. The detached bubble rises and the portion of its volume remaining at the needle becomes the nucleus of the next bubble to form (Expansion stage).

Figure 5 depicts the point extracted coordinates of the interface with respect to time in different stages of bubble growth with equivalent bubble diameter and instantaneous contact angle in each stage. The bubble was produced in a water column with a 15 cm submergence height and a flow rate of 1200 mlph from a needle of 1.6 mm diameter. The equivalent bubble diameter is calculated as the diameter of a sphere that has the same volume as the volume of the bubble at each stage.

The evolution of bubble dimensionless diameter and bubble dimensionless height during the bubble growth is presented in Fig. 6. Bubble dimensionless diameter is defined by the ratio of the equivalent bubble diameter at a specific time to the equivalent bubble detachment diameter. The equivalent bubble detachment diameter is calculated as the diameter of a sphere that has the same volume as the volume of the bubble at the detachment. Similarly, bubble dimensionless height is also determined by the ratio of instantaneous bubble height to the bubble height at the time instance just before the bubble is detached. As shown in Fig. 6, bubble height is defined as the distance between the tip of the needle and the highest point of the bubble.

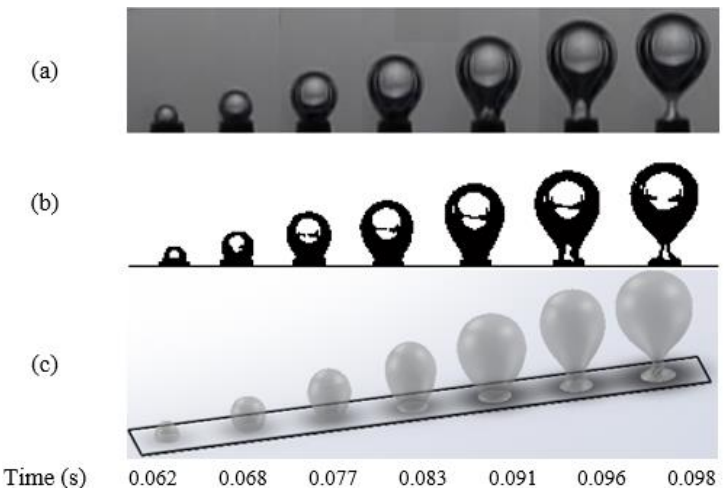

Fig.4. Photographic sequence of bubble growth at 1200 mlph for 1.6 mm diameter needle in distilled water with 15 cm submergence: (a) original image, (b) sequence after image processing, and (c) 3D image

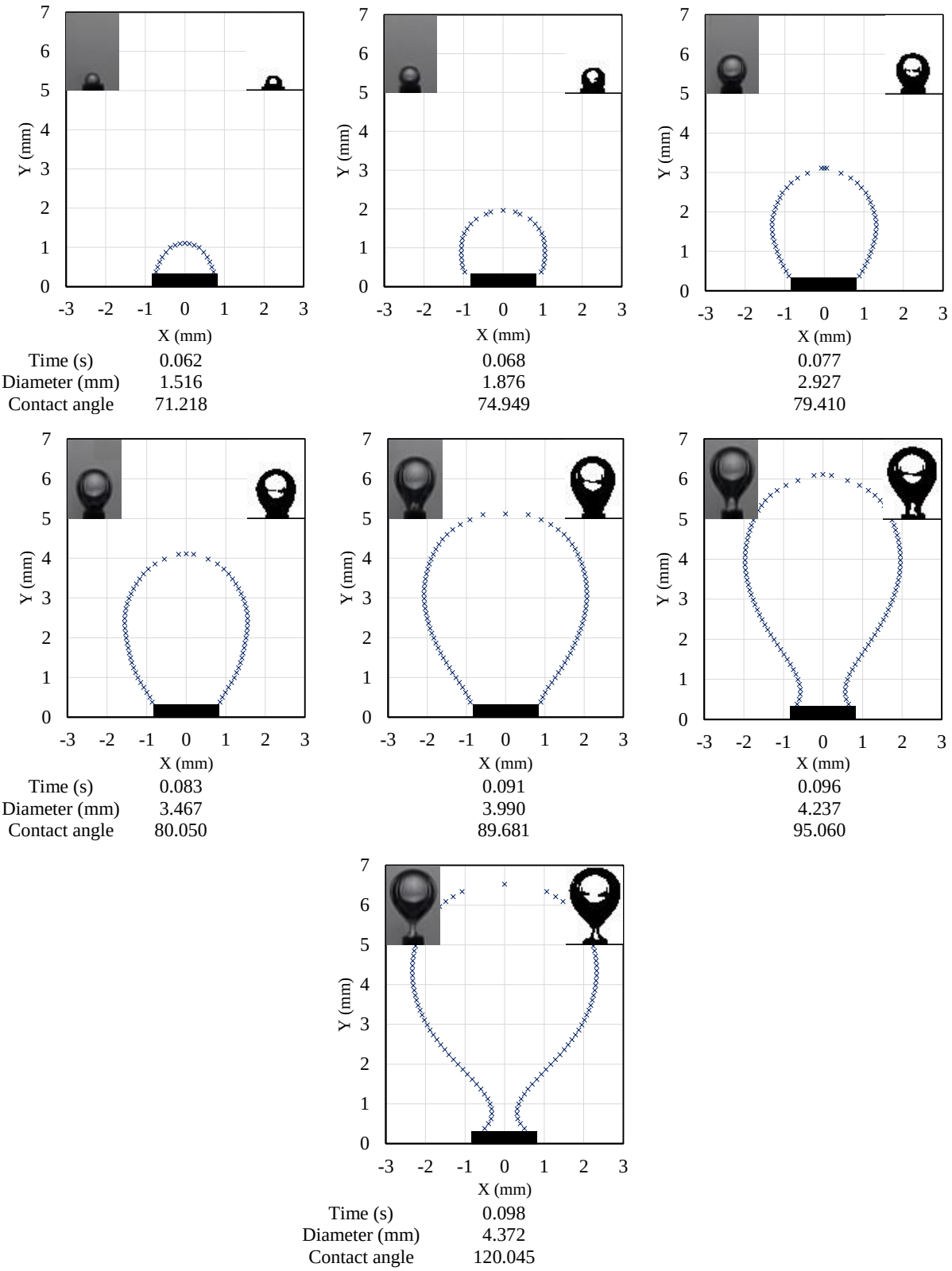

Fig.5. Interface evolution of the generated bubble at 1200 mlph for 1.6 mm diameter needle in distilled water with 15 cm submergence

Three principal stages in bubble growth are illustrated in Fig. 6 and the growth rate at each stage shows the nature of each level. We have obtained that an increase in these two dimensionless parameters in the last part of bubble growth is linear, which is proven in the regression analysis shown in Fig. 6. It should be noted that dimensionless time is designated to the ratio of a particular time over the detachment time. The time of detachment is considered as the time instance, just prior to the bubble pinch-off from the needle. Figure 7 shows the variation of bubble necking length versus the dimensionless time.

Figure 7 illustrates that the necking stage in the bubble growth process is relatively short. Regarding the Fig. 6 and 7, there is a small jump in bubble height at the beginning of the necking stage, as anticipated.

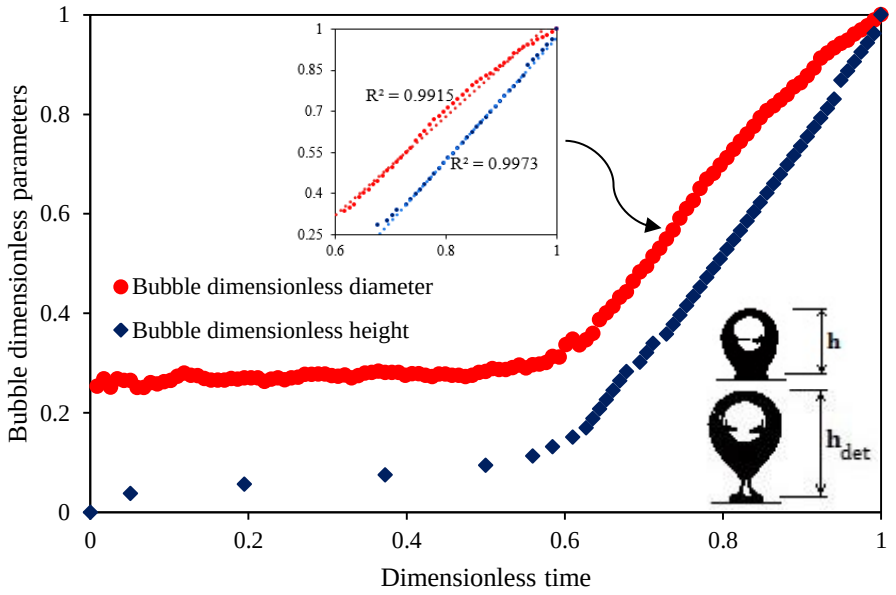

Fig.6. The evolution of bubble dimensionless diameter and height during the bubble growth

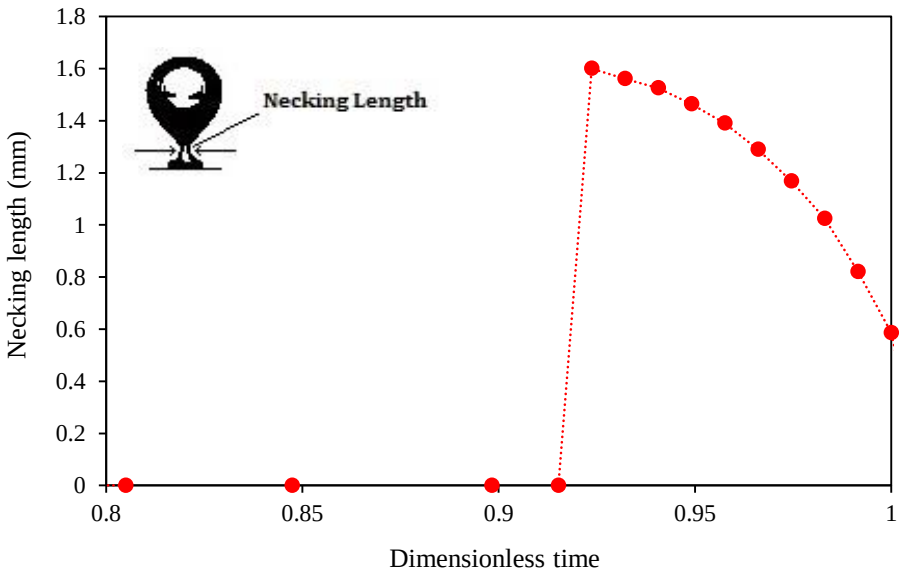

Fig.7. Variation of bubble necking length during the necking stage

Figure 8 also presents the time evolution of the instantaneous contact angle. From the figure, it is possible to clearly identify the three stages of bubble growth based on different behaviors of the contact angle. As the bubble emerges from the needle, the contact angle decreases rapidly and changes from an obtuse angle to an acute one. The partial buoyancy force increases in magnitude until the contact angle reaches a minimum and somewhat steady value of 60 – 75 degree which is more or less maintained during the bubble elongation phase. This phenomena lasts until the partial buoyancy force acting on the upper portion of the bubble is so large that it pulls the bubble dome region upward with enough force to form a neck. As the neck forms, the contact angle increases and once again becomes obtuse as it begins to pinch off which indicates bubble departure.

Figure 8 also shows the instantaneous contact angle sensitivity to the airflow rate. It is obtained that the decreased contact angle is mainly due to a decrease in the magnitude of the partial buoyancy force with the airflow rate. The partial buoyancy force decreases due to the fact that the lower airflow rates yields smaller bubbles. In other words, it is inertial influences in the liquid and gas phases that cause the pressure distribution around the gas-liquid interface to change, thus changing the bubble shape, which therefore influences the partial buoyancy force and contact angle.

Figures 9 and 10 illustrate magnitudes of vertical forces acting on the bubble in different gas flow rates for the bubble produced through the G14 needle in the water column with the submergence height of 15 cm. They also determine the contribution of each force in different operational conditions.

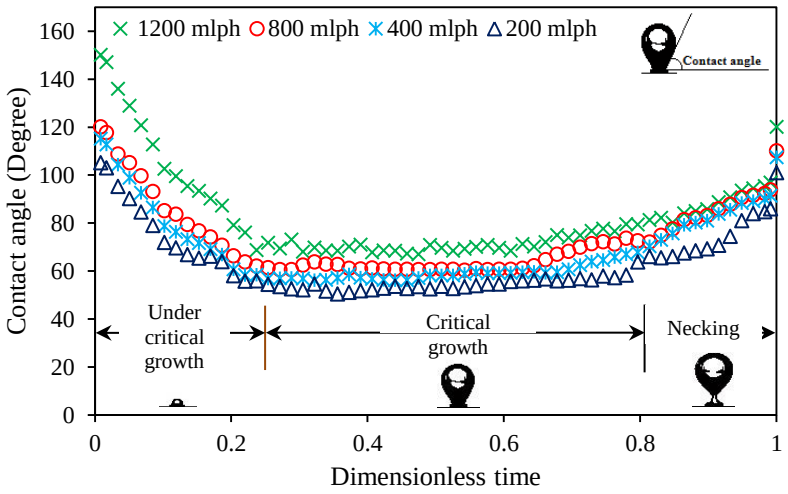

Fig.8. Contact angle evolution at different air flow rates for 1.6 mm diameter needle

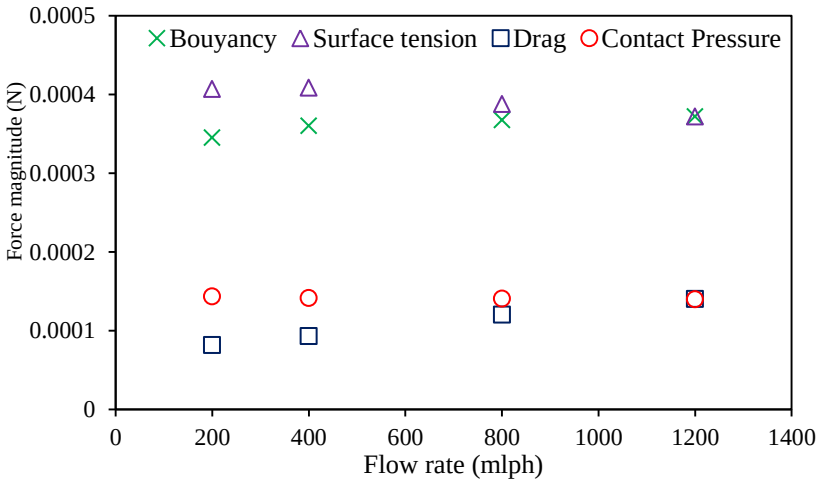

Fig.9. Gas flow rate effect on vertical forces acting on the bubble produced through the injector needle of G14 in water column with the submergence height of 15 cm

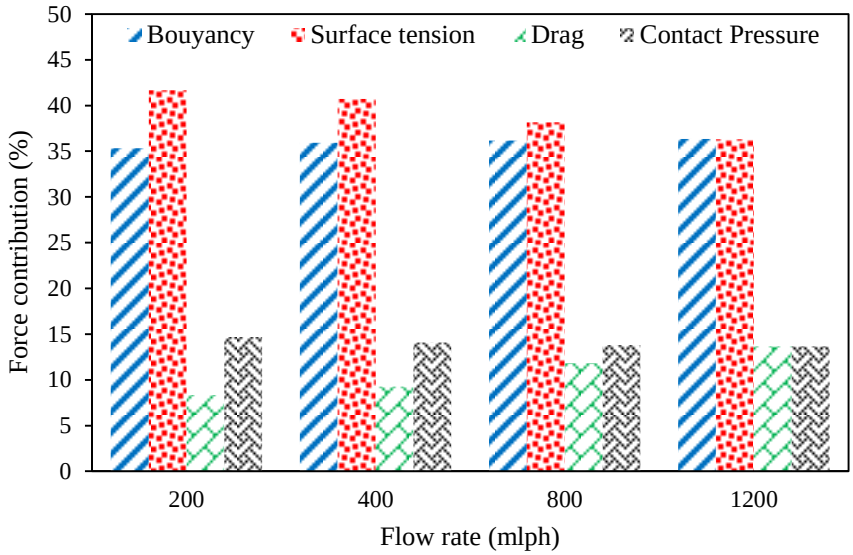

Fig.10. Effect of gas flow rate on each vertical forces contribution for the bubble produced through the injector needle of G14 in water column with the submergence height of 15 cm

Increased buoyancy force with a gas flow rate is the result of an increase in bubble diameter with flow rate, as shown in the above figures. In the case of surface tension force, since an increase in gas flow rate causes an increase in contact angle, the magnitude of this force decreases with the gas flow rate. Regarding Eq. (8) there is an inverse relationship between the magnitude of contact pressure force and bubble diameter; then, it is expectable that contact pressure force decreases with gas flow rate. It is plausible to investigate the changes in the drag coefficient with the gas flow rate in order to develop a deeper understanding of drag force variations with the gas flow rate. To do so, Figure 11 shows the relationship between the drag coefficient and the gas flow rate. Even though the increase in flow rate decreases the drag coefficient, this increase causes an increase in bubble diameter and velocity. So, drag force increases with the gas flow rate due to the dominant effects of bubble diameter and velocity on this force.

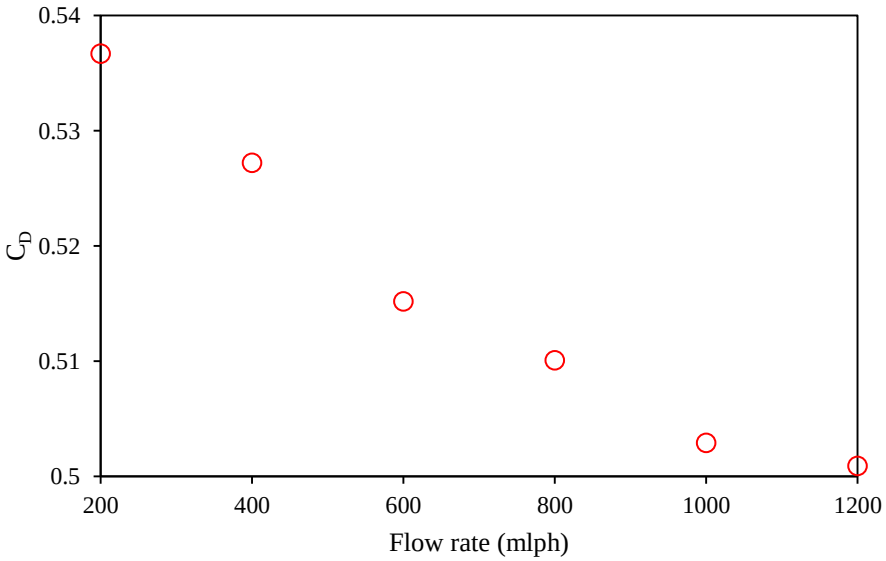

Fig.11. Changes in drag coefficient with gas flow rate for the bubble produced through the injector needle of G14 in water column with the submergence height of 15 cm

4.2. Sensitivity analysis of bubble departure characteristics

In this section, an investigation will be done on the equivalent bubble detachment diameter and bubble generation frequency sensitivity to the operational parameters. These effective parameters can be grouped into three categories: Liquid properties (liquid column height and liquid viscosity), airflow rate, and injection specification (needle diameter and submergence type—vertical and horizontal needle). All results are presented for vertical needle injection to discover the effect of each parameter,. Also, at the end of this section, vertical and horizontal results will be compared to clarify the effect of submergence type. Figure 12 shows the effects of liquid viscosity, needle diameter, airflow rate, and submergence height on the equivalent bubble detachment diameter. Figure 12(a) depicts the effects of submergence height in the water column with the injector needle of G14, Fig. 12(b) presents the liquid viscosity effects with the injector needle of G14 and 15 cm liquid height and Fig. 12(c) shows the needle diameter effects in the silicon oil column (viscosity of 0.1 Pa.s) with a height of 15 cm. It should be noted that all three figures can be used to determine the airflow rate effects on bubble detachment diameter.

To analyze the results shown in Fig. 12 and other bubble detachment characteristics, it is necessary to pay attention to the governing forces controlling the bubble detachment features in conjunction with force balancing analysis presented in Section 4.1. Generally, for downward forces, surface tension is the dominant force during bubble formation. Buoyancy is always a dominant upward force at departure, except at very large Bond numbers where contact pressure force may be dominant. In this case, three significant forces that mostly govern the bubble detachment size are surface tension, drag, and buoyancy forces. Balancing between these three items in different operational conditions controls the bubble size. Surface tension force is significant in cases where needle diameter is larger, especially in the low gas flow regime injections. On the other hand, the buoyancy force is considerable in conditions with a higher gas flow rate and smaller needle diameter.

Considering the above introductory explanation, it is predictable to have a larger bubble detached from needles with a larger diameter, as it is observed from Fig. 12(c). In addition, it is well known that bubbles depart the needles larger in higher gas flow rates (Fig. 12). It should be considered that drag force in higher gas flow rates is one of the significant forces and that it plays an important role in the determination of the bubble detachment diameter especially in high viscosity liquids. In high gas flow rate regimes, the drag coefficient is critical and in direct relation to bubble diameter.

Additionally, as the Reynolds number is the ratio of momentum forces to viscous forces, by increasing in liquid viscosity, smaller Reynolds numbers are achieved that the bubble drag coefficient is inversely proportional to the Reynolds number. In other words, higher viscosity of liquid results in a higher drag coefficient in drag force and, consequently, larger bubbles at departure, as seen in Fig. 12(b). Since the differences in bubble detachment diameter at a flow rate of 1200 mlph is larger than those at 400 or 200 mlph, liquid viscosity plays a more important role in higher gas flow rates. Also, regarding the liquid viscosity effects, higher bubble sphericity in viscous liquids results in larger bubbles due to an increase in the injected area and the drag force.

Figure 13 shows the effects of liquid viscosity, needle diameter, airflow rate, and submergence height on the bubble generation frequency. Figure 13(a) depicts the effects of submergence height in the water column with the injector needle of G14, Fig. 13(b) presents the liquid viscosity effects with the injector needle of G14 and 15 cm liquid height and Fig. 13(c) shows the needle diameter effects in the silicon oil column (viscosity of 0.1 Pa.s) with a height of 15 cm. It should be noted that all three figures can be used to determine the airflow rate effects on bubble generation frequency.

As it was previously mentioned, the air is injected into the liquid column at constant flow rates and due to this critical operational condition, there will be a reverse relation between bubble departure diameter and bubble generation frequency. In other words, in a constant airflow rate, increased needle diameter results in a smaller number of bubbles produced at a particular time. Also, by increasing the liquid viscosity, the bubble

generation frequency will be increased at a constant airflow injection rate. As it is observed, in a liquid column with higher submergence height at a constant airflow rate, the number of the generated bubbles at a particular time is increased. Furthermore, finally, as it is predictable, higher airflow rates, increase the bubble generation frequency.

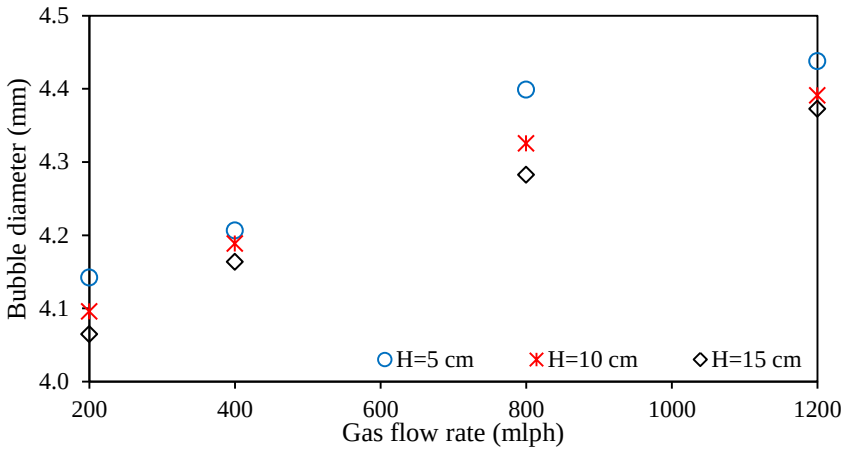

(a)

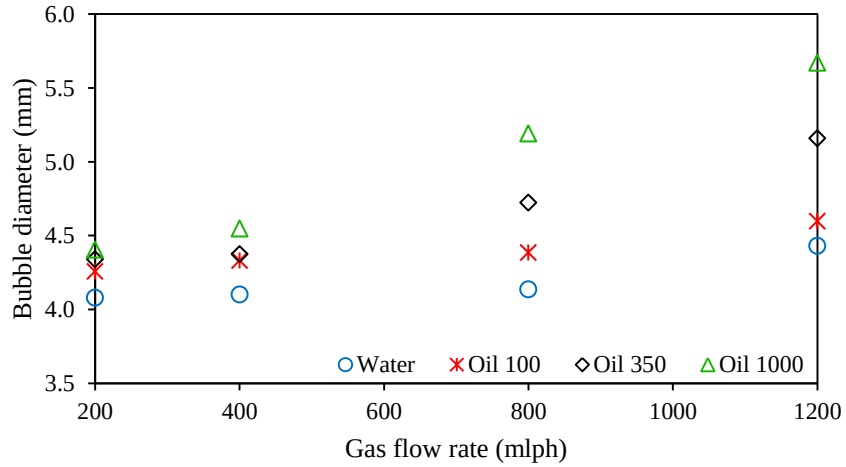

(b)

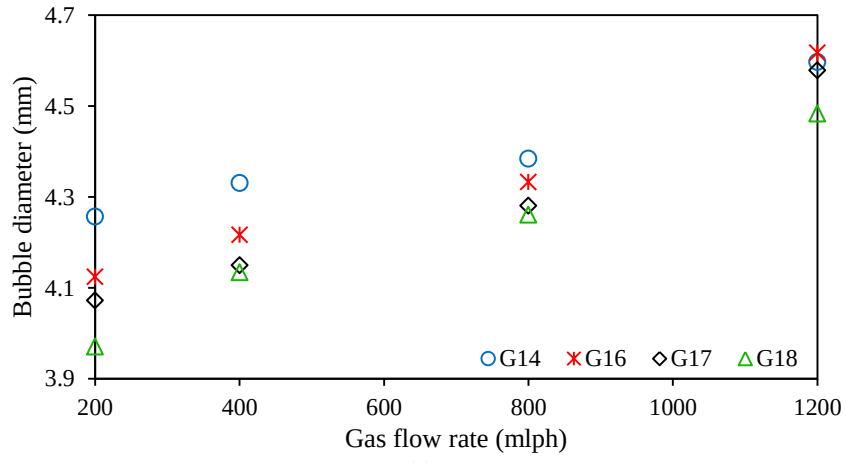

(c)

Fig.12. Variation of bubble detachment diameter at different operating conditions: (a) submergence height effects in water column with the injector needle of G14, (b) liquid viscosity effects with the liquid height of 15 cm and the injector needle of G14, and (c) needle diameter effects in silicon oil 100 column with the submergence height of 15 cm

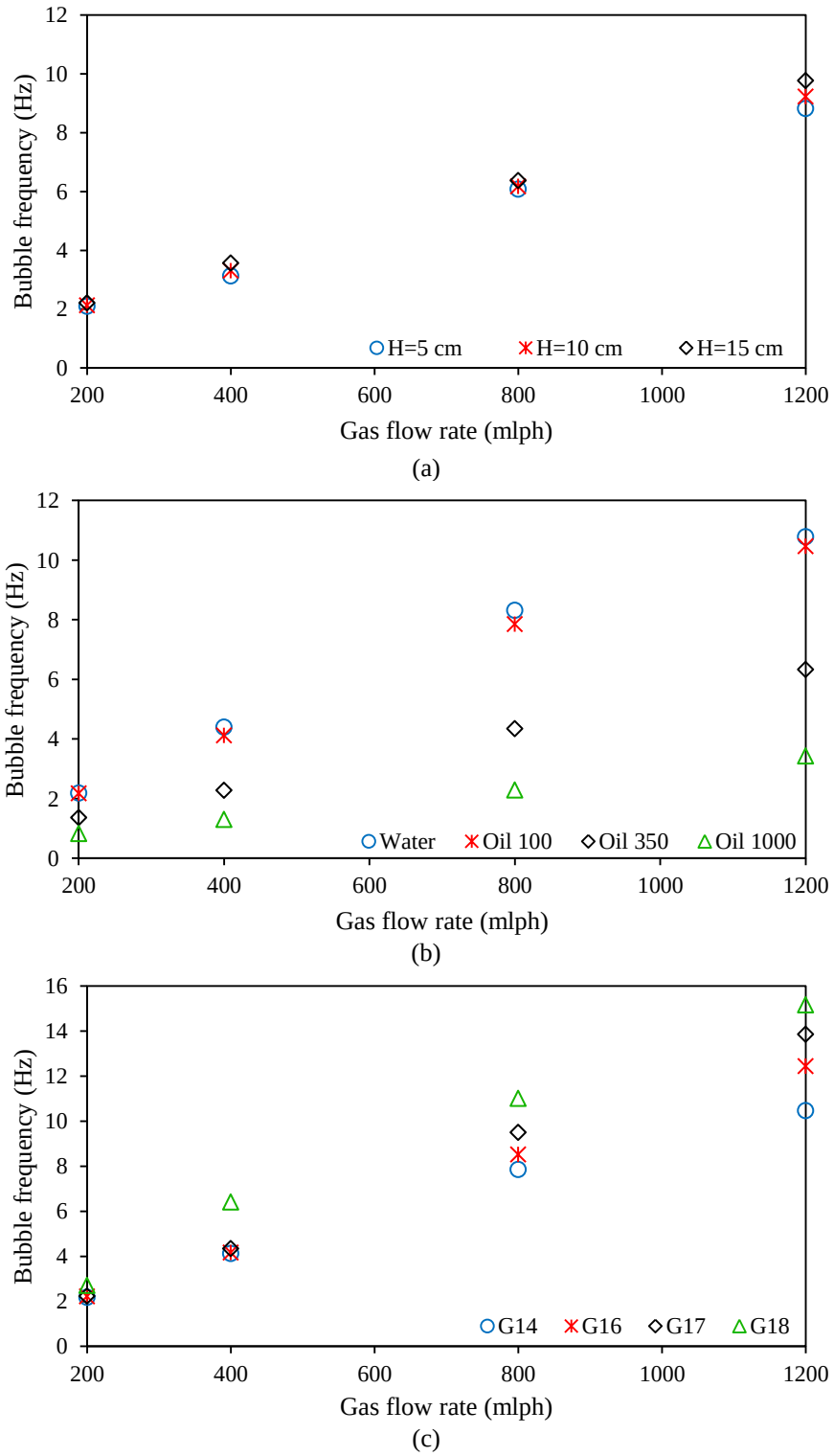

Fig.13. Variation of bubble generation frequency in different operational condition: (a) submergence height effects in water column with the injector needle of G14, (b) liquid viscosity effects with the water height of 15 cm and the injector needle of G14, and (c) needle diameter effects in silicon oil 100 column with the submergence height of 15 cm

To have a clear understanding, the extracted point coordinates of the bubble interface are presented for different operational conditions to find out the effects of these parameters on bubble detachment diameter and shape. Figure 14(a) demonstrates the impacts of airflow rate on the bubble detachment shape and diameter. These bubbles were produced in water with the submergence height of 15 cm and the injector needle of G14. Figure 14(b) depicts the needle diameter effects on the bubble departure characteristics in a liquid column with a height of 15 cm and an airflow rate of 1200 mlph. Figure 14(c) presents the effects of submergence height on the bubble detachment shape and diameter in the water column with an injector needle of G14 and the airflow rate of 1200 mlph.

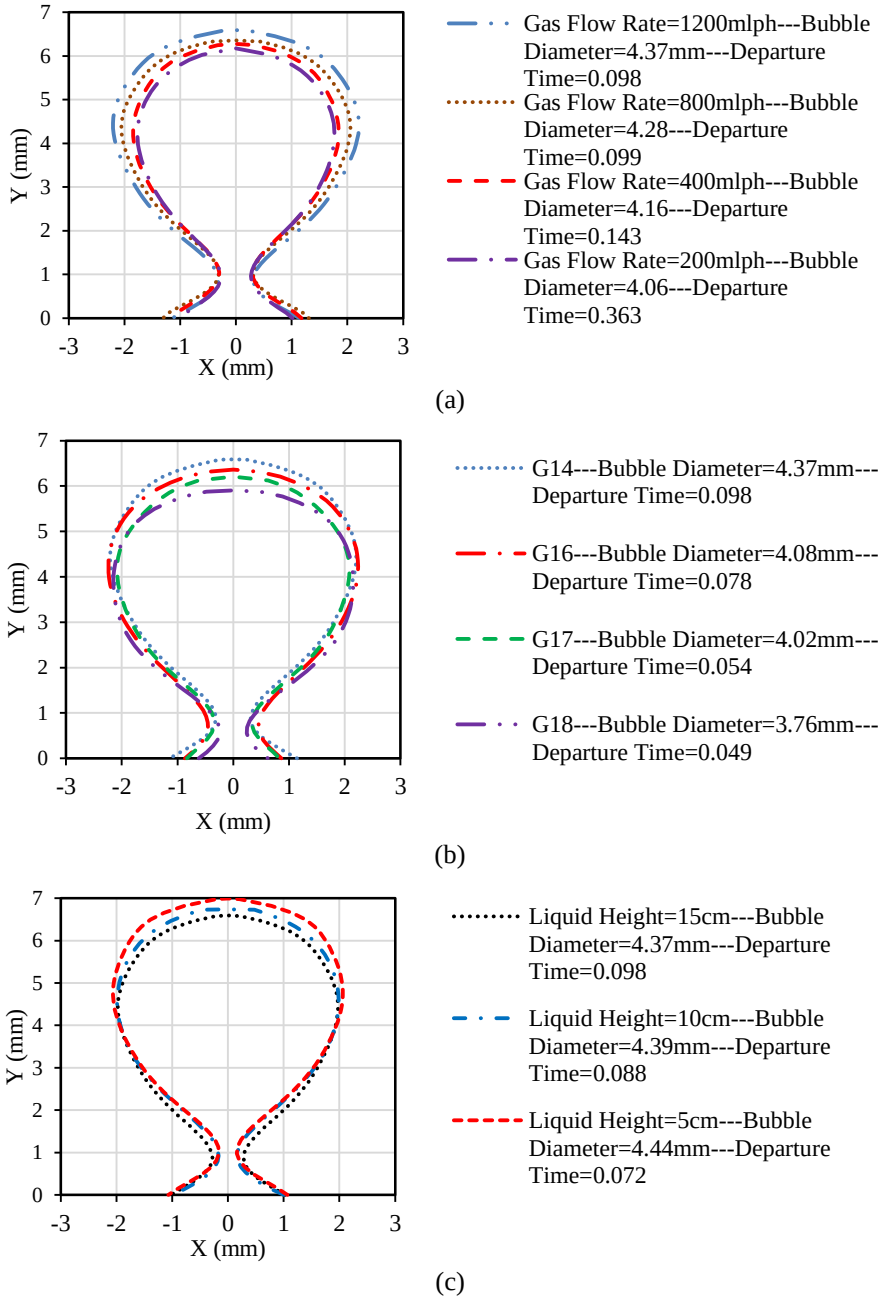

Fig.14. Bubble detachment characteristics in different operational conditions in the water column: (a) effects of gas flow rate with 15 cm submergence height and the injector needle of G14, (b) effects of needle diameter with 15 cm submergence height and the air flow rate of 1200 mlph, and (c) submergence height effects with the air flow rate of 1200 mlph and the G14 needle

As seen in Fig. 14, increased needle diameter and gas flow rate, and decreased submergence height results in a larger bubble at the departure due to causes clarified previously. A needle can be submerged in three ways: top submergence, bottom submergence, and side submergence. To discover the effects of submergence types, in identical conditions, bubbles are produced in a water bubble column from vertical and horizontal oriented needles. In both cases, the air is injected through the needle (with an inner diameter of 1.6 mm) into the water column of 15 cm height with a flow rate of 1200 mlph. Figure 15 shows the comparison between the bubble detachment diameter and bubble generation frequency of the bubbles produced from these two types of injection systems.

Figure 15 indicates that there is not much difference in bubble detachment characteristics in these two different types of injection systems. Also, the effects of submergence type in bubble detachment diameter and bubble generation frequency can be ignored in the mentioned operational conditions in this study (could be different for below-critical injection flow rates). It can be easily seen from the comparison between the forces acting on a single bubble during growth and detachment stage that there is no significant difference in forces exerted on the bubble produced through vertical or horizontal needles. Drag, surface tension, virtual mass, buoyancy, and gravity forces can be considered as the fundamental forces in the bubble growth process in a stagnant liquid. One of the distinctions between vertical and horizontal injections is the direction of gas momentum delivered to the bubble. Considering the nature of this item in the bubble formation process indicates that gas momentum in vertical or horizontal directions has no role in bubble detachment diameter. Therefore, it is acceptable to expect identical results in both vertical and horizontal injection systems for bubble detachment characteristics, as can be seen in Fig. 15.

4.3. Neural Network Analysis

Over the past decade, significant advances in recognition of the structure and mechanisms of the brain for encountering complicated scientific, have led to the development of Artificial Neural Network (ANN). Neural networks are composed of simple, highly interconnected processing elements inspired by neurons operating in parallel. This structure enables ANN to be capable of learning the non-linear relations between a set of inputs and outputs.

In this study, a multilayer feed-forward backpropagation ANN model has been developed to train the network. The most commonly used method for mapping sets of input data into a set of appropriate outputs in mechanical and chemical engineering applications is the multilayer perceptron (MLP). This method utilizes the supervised learning technique that consists of input and output layers, and at least one layer of processing units called hidden layer.

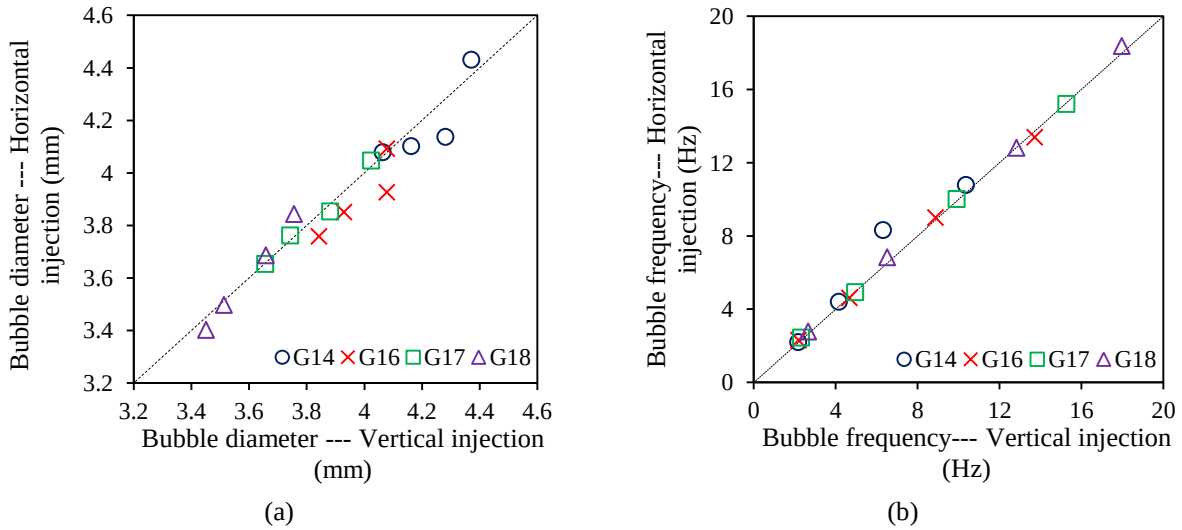

(a) (b)

Fig.15. Comparison between the bubble detachment characteristics of the bubbles produced from horizontal and vertical injectors: (a) equivalent bubble detachment diameter, and (b) bubble generation frequency

The schematic diagram of the neural network model applied in this study is shown in Fig.16. MATLAB neural network toolbox was used to design the network model. The present network model consists of an input layer with five neurons (surface tension, viscosity, orifice diameter, gas flow rate, and liquid column height), an output layer of one neuron (bubble detachment diameter), and a hidden layer of ten neurons.

As a first step, the neural network model randomly partitions the experimental data off into three sets, in which 65 percent of data are chosen to train the network model and 20 percent of the data are opted to validate the network integrity and finally the remaining data are used for testing the network robustness after validation. Figure 17 shows the performance graph of the neural network model. It is observed that the desired goal has been reached by minimization of performance function, i.e., MSE with performance level 5×10^{-4} in 22 epochs.

When the neural network model is trained, the most important remaining task is to determine how well the network predicts the output results. Checking the performance of a trained network involves the regression analysis and calculating mean squared error for experimental data and network outputs. Figure 18 depicts the consistency of the collected and predicted results.

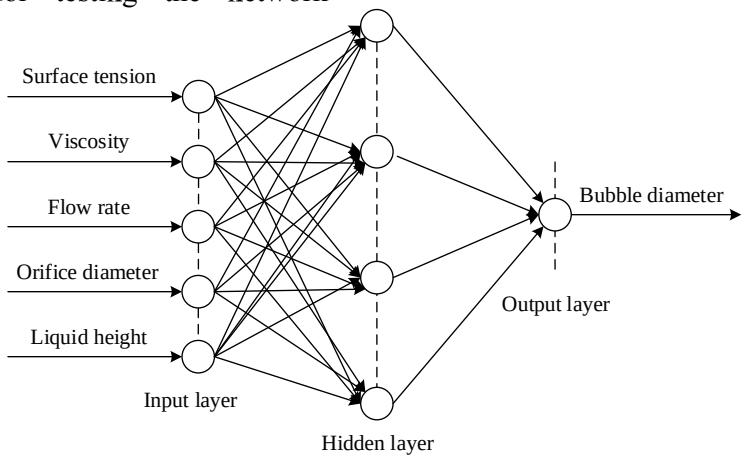

Fig.16. Artificial neural network structure

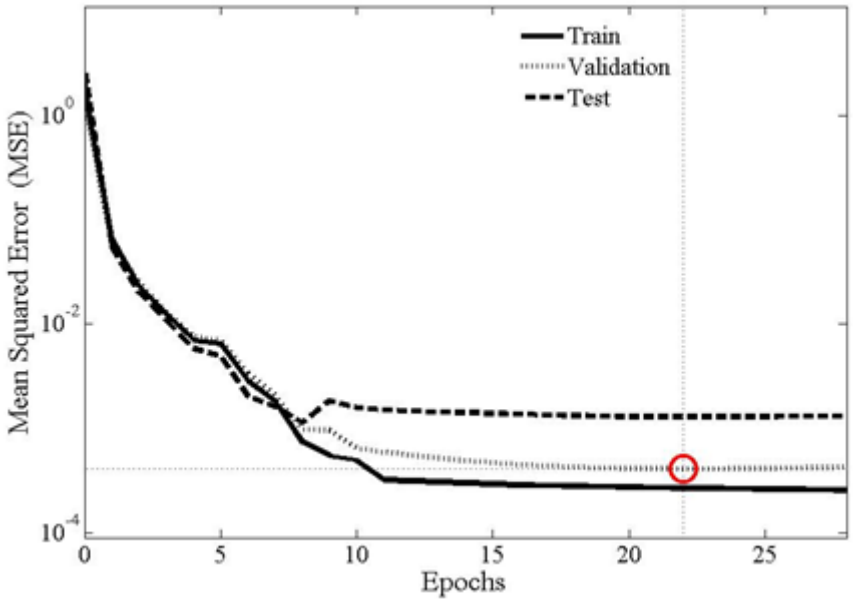

Fig.17. Network performance graph

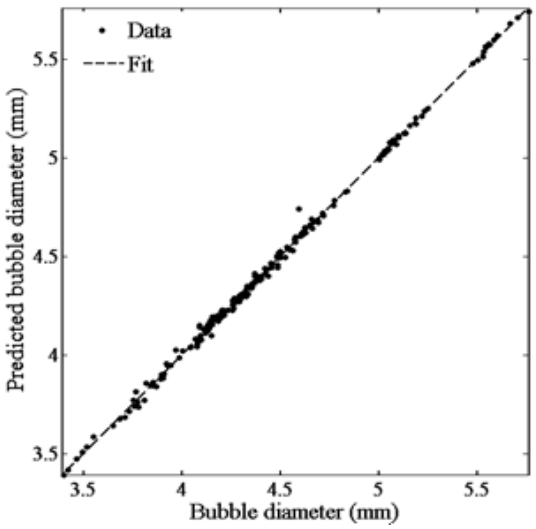

Fig.18. Comparison between experimental data and artificial neural network outputs (Regression = 0.99908, MAE = 0.017, and MSE = 0.00041015)

4.4.Parametric Correlation

As the process of bubble generation in a liquid column includes a large number of parameters, the experimental results are correlated empirically using dimensional analysis. The Buckingham theorem was used for finding appropriate dimensionless groups for this problem, and the new empirical correlation was developed. The bubble departure diameter depends on the following dimensional variables: liquid density, liquid dynamic viscosity, surface tension, orifice diameter, gas flow rate, liquid height from the injector, and the gravitational acceleration. That is,

$$F[\rho_L.g.d_O.\sigma.\mu_L.Q.d_B.h] \equiv 0. \quad (10)$$

This equation consists of eight variables with three basic primary dimensions needed to express the variables, which are mass (M) in kilogram, length (L) in meter, and time (T) in second. Based on the above, the number of dimensionless variables applicable to this problem is five. By using a step-by-step approach, the three prime variables are selected, and another five repeated variables are found. That is,

$$F[\pi_1.\pi_2.\pi_3.\pi_4.\pi_5] \equiv 0\,. \quad (11)$$

This method yields some dimensionless groups of parameters in which the experimental data have been combined. The variables in the study formulated into dimensionless numbers consist of the Bond number, Froude number, Galileo number, ratio of liquid height over orifice diameter, and diameter ratio. It must be noted that based on the Stokes' law, Reynolds number has a negligible effect on this study; therefore, it was not considered as an effective dimensionless number. Hence,

$$\pi_1 = Bd = \frac{\rho_L g {d_O}^2}{\sigma}\ (Bond\ number), \quad (12)$$

$$\pi_2 = Fr = \frac{16Q^2}{g\pi^2 {d_O}^5}\ (Froude\ number), \quad (13)$$

$$\pi_3 = Ga = \frac{g{\rho_L}^2 {d_O}^3}{{\mu_L}^2}\ (Galileo\ number), \quad (14)$$

$$\pi_4 = \frac{h}{d_O} \quad (15)$$

$$\left(\begin{matrix}Ratio\ of\ liquid\ height\ to \\ orifice\ diameter\end{matrix}\right)$$

and

$$\pi_5 = \frac{d_B}{d_O}\ (Diameter\ ratio). \quad (16)$$

The parametric correlation can be acquired by superimposing the four independent dimensionless numbers for the low, medium, and high gas flow rates as follows:

$$\frac{d_B}{d_O} = \left[a_1 Bd^{b_1} + a_2 Ga^{b_2} Fr^{b_3} + a_3 Fr^{b_4}\left(\frac{h}{d_O}\right)^{b_5}\right]^{b_6}. \quad (17)$$

The values of the constants are estimated using MATLAB optimization toolbox. The effectiveness of the correlation is judged by the mean absolute error (MAE). Thus, for the development of the correlation, the error between correlation results and experimental data was minimized. The obtained correlation is, hence, given by

$$\frac{d_B}{d_O} = \left[7.08Bd^{-0.079} + 2.242Ga^{-0.05}Fr^{0.07} + 0.894Fr^{-1.868}\left(\frac{h}{d_o}\right)^{-1.933}\right]^{3.604}. \quad (18)$$

The mean absolute percentage error between predicted and experimental data is 8 %, which demonstrates the accuracy of the developed correlation. The deviation of correlation values from the experimental results is demonstrated in Fig. 19. This figure also shows the comparison of the achieved correlation in the present investigation and one of the most accurate published correlations from Jamialahmadi et al. [18] article. It is understandable from the figure that the correlation of the mentioned article has a considerable difference to experimental observations. The main reason that can be presented for this deviation is ignoring the submergence height, as a remarkable parameter, in Jamialahmadi's correlation.

Now, it is possible to investigate the dependence of bubble detachment diameter upon dimensionless numbers defined earlier. To do so, Fig. 20 depicts the variation of diameter ratio (ratio of bubble detachment diameter to orifice diameter) with Froude number, Galileo number, Bond number, and height ratio (ratio of submergence height to orifice diameter). In other words, Fig. 20 is a sensitivity analysis of bubble detachment diameter on dimensionless numbers defined earlier.

It is discovered that the most significant factor that controls the bubble detachment characteristics is Bond number, as expected regarding the analysis provided in sections 4.1 and 4.2. In other words, the bubble detachment diameter is more sensitive to the small variation in Bond number in comparison with other dimensionless numbers. This number, which characterizes the bubble shape, shows the importance of surface tension and density difference between the gas bubble and surrounding fluid. The less effective dimensionless parameter on bubble detachment diameter is the Froude number. This number expresses the importance of gas flow rate and orifice diameter and is used in defining the Morton number which characterizes the bubble shape.

Moreover, the least important parameters in the bubble hydrodynamics study are Galileo number and the height ratio. It is determined that the bubble detachment characteristics are not affected by height ratio especially for values more than 50 and this is the cause of ignoring this parameter in most studies. It should be mentioned that this analysis is valid for operating conditions mentioned in this study, and in the ranges far from the mentioned conditions, further investigations are necessary.

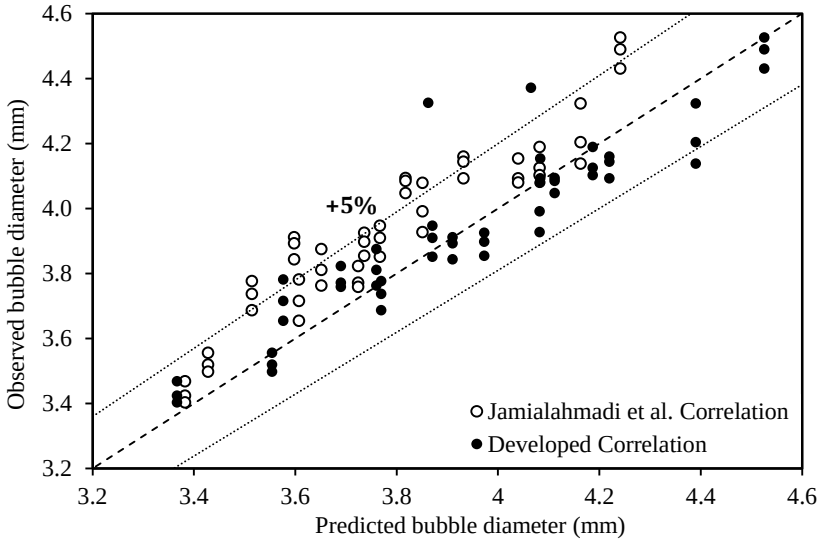

Fig.19. Comparison of measured bubble diameter with correlation predicted values (Developed correlation – MAE = 0.08; Jamialahmadi et al. – MAE = 0.15) Notes: The region between the left dotted line and dashed line represents the underestimation region with less than 5% error and the region between the right dotted line and dashed line shows the overestimation error with less than 5% error

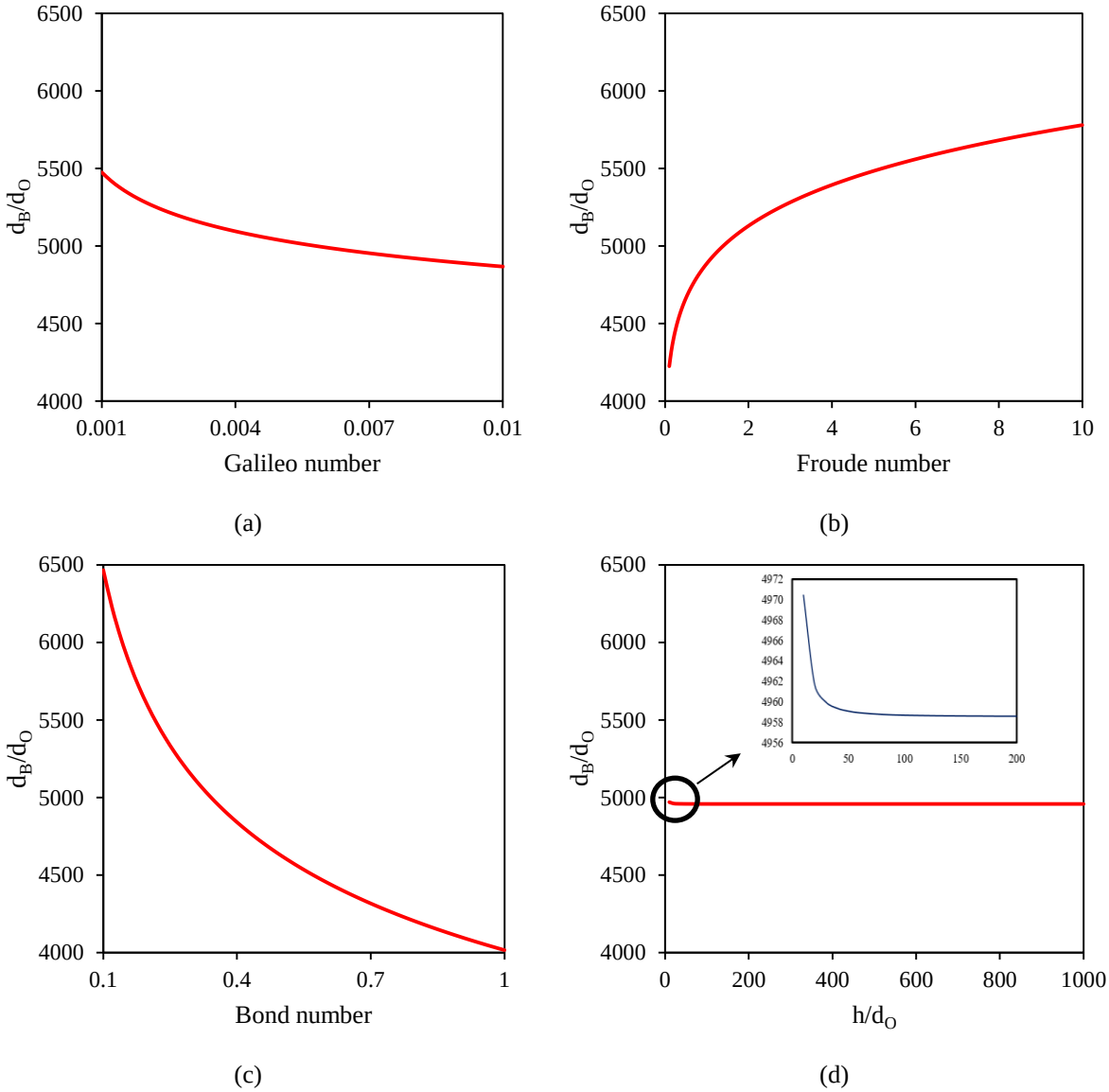

Fig.20. Sensivity analysis of bubble diameter at detachment on dimensionless numbers: a) Galileo number, (b) Froude number, c) Bond number, d) height ratio

4. Conclusion

In this study, an experimental investigation on the air bubble formation, growth, and detachment in a stagnant liquid column was performed using a high-speed video-imaging system and digital image processing. Experiments were performed at low airflow rates (200 – 1200 mlph) through four needles with different diameters in four different liquids and three different submergence heights. To evaluate the effects of submergence type (vertical or horizontal injection systems), experiments were done for both injection systems. The bubble detachment characteristics and bubble generation frequency were correlated with all controlling parameters using feed-forward back propagation neural network architecture. The experimental data also used to develop a new correlation to predict the bubble detachment diameter. The mean absolute error between the proposed correlation and experimental data was approximately ±8%. For the wide range of experimental conditions applied in this study, the following was concluded:

- The submergence type (vertical or horizontal injection system) had no significant effect on the bubble detachment characteristics in the

mentioned operational conditions in this study

- The increase in needle diameter, liquid viscosity, and gas flow rate resulted in a larger bubble at the departure
- For bubble formation under constant flow condition, the effect of controlling parameters on bubble detachment diameter and bubble generation frequency were inverse
- Due to buoyancy force effects, the bubble contact angles decreased by increasing airflow rate
- The effect of surface tension force was found to be significant on the bubble size, especially for large needle diameters and at low gas flow rates
- The buoyancy force was found to significantly affect the bubble size at higher gas flow rates and smaller needle diameters. On the other hand, the effect of viscosity on bubble detachment characteristics was more dominant at the same conditions.
- The artificial neural network was found to estimate the bubble diameter in various conditions (MAE = 0.017), and the developed correlation was able to predict the bubble size with reasonable accuracy.

References

[1] Ghofrani, Ali, Seyyed Danial Nazemi, and Mohsen A. Jafari. "HVAC load synchronization in smart building communities." Sustainable Cities and Society 51 (2019): 101741.

[2] Kosari, Erfan, Ali Rahnama, Mahyar Momen, Pedram Hanafizadeh, and Mohammad Mahdi Rastegardoost. "Drag coefficient and Strouhal number analysis of a rectangular probe in a two-phase cross-flow." Energy Equipment and Systems 6, no. 1 (2018): 7-15.

[3] Baniassadi, Amir, Mahyar Momen, Mehrdad Shirinbakhsh, and Majid Amidpour. "Application of R-curve analysis in evaluating the effect of integrating renewable energies in cogeneration systems." Applied thermal engineering 93 (2016): 297-307.

[4] Rollbusch, Philipp, Marc Becker, Martina Ludwig, Andrè Bieberle, Marcus Grünewald, Uwe Hampel, and Robert Franke. "Experimental investigation of the influence of column scale, gas density, and liquid properties on gas holdup in bubble columns." International Journal of Multiphase Flow 75 (2015): 88-106.

[5] Besagni, Giorgio, Pietro Brazzale, Alberto Fiocca, and Fabio Inzoli. "Estimation of bubble size distributions and shapes in a two-phase bubble column using image analysis and optical probes." Flow Measurement and Instrumentation 52 (2016): 190-207.

[6] Adetunji, Olubode, and Randhir Rawatlal. "Estimation of bubble column hydrodynamics: Image-based measurement method." Flow Measurement and Instrumentation 53 (2017): 4-17.

[7] Tate, Thomas. "XXX. On the magnitude of a drop of liquid formed under different circumstances." The London, Edinburgh, and Dublin Philosophical Magazine and Journal of Science 27, no. 181, (1864): 176-180.

[8] Satyanarayan, A., R. Kumar, and N. R. Kuloor. "Studies in bubble formation—II bubble formation under constant pressure conditions." Chemical Engineering Science 24, no. 4 (1969): 749-761.

[9] Gerlach, D., G. Biswas, F. Durst, and V. Kolobaric. "Quasi-static bubble formation on submerged orifices." International Journal of Heat and Mass Transfer 48, no. 2 (2005): 425-438.

[10] Zhang, Lei, and Masahiro Shoji. "Aperiodic bubble formation from a submerged orifice." Chemical Engineering Science 56, no. 18 (2001): 5371-5381.

[11] Sada, Eizo, Akira Yasunishi, Shigeo Katoh, and Masashi Nishioka. "Bubble formation in flowing liquid." The Canadian Journal of Chemical Engineering 56, no. 6 (1978): 669-672.

[12] Prosperetti, A., and A. Lezzi. "Bubble dynamics in a compressible liquid. Part 1. First-order theory." Journal of Fluid Mechanics 168 (1986): 457-478.

[13] Georgoulas, Anastasios, P. Koukouvinis, Manolis Gavaises, and Marco Marengo. "Numerical investigation of quasi-static bubble growth and detachment from submerged orifices in isothermal liquid pools: The effect of varying fluid properties and

gravity levels." International Journal of Multiphase Flow 74 (2015): 59-78.
[14] Oguz, Hasan N., and Andrea Prosperetti. "Dynamics of bubble growth and detachment from a needle." Journal of Fluid Mechanics 257 (1993): 111-145.
[15] Leibson, Irving, Eugene G. Holcomb, Anthony G. Cacoso, and John J. Jacmic. "Rate of flow and mechanics of bubble formation from single submerged orifices. I. Rate of flow studies." AIChE Journal 2, no. 3 (1956): 296-300.
[16] Benzing, Robert J., and John E. Myers. "Low-frequency bubble formation at horizontal circular orifices." Industrial & Engineering Chemistry 47, no. 10 (1955): 2087-2090.
[17] Khurana, A. K., and Rajinder Kumar. "Studies in bubble formation—III." Chemical Engineering Science 24, no. 11 (1969): 1711-1723.
[18] Jamialahmadi, M., M. R. Zehtaban, H. Müller-Steinhagen, A. Sarrafi, and J. M. Smith. "Study of bubble formation under constant flow conditions." Chemical Engineering Research and Design 79, no. 5 (2001): 523-532.
[19] Eshraghi, J., E. Kosari, P. Hadikhani, A. Amini, M. Ashjaee, and P. Hanafizadeh. "Numerical study of surface tension effects on bubble detachment in a submerged needle." WIT Transactions on Engineering Science (2015): 77-86.
[20] Liow, Jong-Leng. "Quasi-equilibrium bubble formation during top-submerged gas injection." Chemical Engineering Science 55, no. 20 (2000): 4515-4524.
[21] Hsu, Shu-Hao, Wei-Hua Lee, Yu-Min Yang, Chien-Hsiang Chang, and Jer-Ru Maa. "Bubble formation at an orifice in surfactant solutions under constant-flow conditions." Industrial & engineering chemistry research 39, no. 5 (2000): 1473-1479.
[22] Idogawa, K., K. Ikeda, T. Fukuda, and S. Morooka. "Formation and flow of gas bubbles in a pressurized bubble column with a single orifice or nozzle gas distributor." Chemical Engineering Communications 59, no. 1-6 (1987): 201-212.
[23] Davidson, Leon, and Erwin H. Amick. "Formation of gas bubbles at horizontal orifices." AIChE Journal 2, no. 3 (1956): 337-342.
[24] Wilkinson, Peter Mervyn. "Physical aspects and scale-up of high-pressure bubble columns." Ph.D. diss., Rijksuniversiteit Groningen, 1991.
[25] Hanafizadeh, P., J. Eshraghi, E. Kosari, and W. H. Ahmed. "The effect of gas properties on bubble formation, growth, and detachment." Particulate Science and Technology 33, no. 6 (2015): 645-651.
[26] Dietrich, Nicolas, Nadia Mayoufi, Souhil Poncin, and Huai-Zhi Li. "Experimental investigation of bubble and drop formation at submerged orifices." Chemical Papers 67, no. 3 (2013): 313-325.
[27] Di Bari, Sergio, and Anthony J. Robinson. "Experimental study of gas injected bubble growth from submerged orifices." Experimental Thermal and Fluid Science 44 (2013): 124-137.
[28] Badam, V. K., V. Buwa, and F. Durst. "Experimental investigations of regimes of bubble formation on submerged orifices under constant flow condition." The Canadian Journal of Chemical Engineering 85, no. 3 (2007): 257-267.
[29] Davidson, J. F. "Bubble formation at an orifice in a viscous liquid." Transaction of Institute of Chemical Engineering 38 (1960): 144-154.
[30] Ramakrishnan, S., R. Kumar, and N. R. Kuloor. "Studies in bubble formation—I bubble formation under constant flow conditions." Chemical Engineering Science 24, no. 4 (1969): 731-747.
[31] Iliadis, Prodromos, Vasilios Douptsoglou, and Michael Stamatoudis. "Effect of orifice submergence on bubble formation." Chemical Engineering & Technology: Industrial Chemistry-Plant Equipment-Process Engineering-Biotechnology 23, no. 4 (2000): 341-345.
[32] Vafaei, Saeid, Panagiota Angeli, and Dongsheng Wen. "Bubble growth rate from stainless steel substrate and needle nozzles." Colloids and Surfaces A: Physicochemical and Engineering Aspects 384, no. 1-3 (2011): 240-247.
[33] Houshmand, Farzad, Daren Elcock, Michael Amitay, and Yoav Peles. "Bubble formation from a micro-pillar

in a microchannel." International Journal of Multiphase Flow 59 (2014): 44-53.
[34] Winterson, R. H. S. "A simple method of predicting bubble size in bubble columns." Chemical Engineering and Processing: Process Intensification 33, no. 1 (1994): 1-5.
[35] Akita, Kiyomi, and Fumitake Yoshida. "Bubble size, interfacial area, and liquid-phase mass transfer coefficient in bubble columns." Industrial & Engineering Chemistry Process Design and Development 13, no. 1 (1974): 84-91.
[36] Lesage, Frédéric J., James S. Cotton, and Anthony J. Robinson. "Modelling of quasi-static adiabatic bubble formation, growth, and detachment for low Bond numbers." Chemical Engineering Science 104 (2013): 742-754.
[37] Lesage, Frédéric J., James S. Cotton, and Anthony J. Robinson. "Analysis of quasi-static vapour bubble shape during growth and departure." Physics of Fluids 25, no. 6 (2013): 067103.
[38] Lesage, Frédéric J., and Francis Marois. "Experimental and numerical analysis of quasi-static bubble size and shape characteristics at the detachment." International Journal of Heat and Mass Transfer 64 (2013): 53-69.
[39] Morrison, Faith A. "Data correlation for drag coefficient for a sphere." Department of Chemical Engineering, Michigan Technological University, Houghton, MI 49931 (2013).